Progress In Electromagnetics Research, Vol. 108, 51–64, 2010

GENERALIZED SYNTHESIS OF RAT RACE RING COUPLER AND ITS APPLICATION TO CIRCUIT MINIATURIZATION

J.-T. Kuo

Department of Electronic Engineering
Chang Gung University
Taoyuan, Taiwan

C.-H. Tsai

Institute of Communication Engineering
National Chiao Tung University
Hsinchu, Taiwan

Abstract—Generalized synthesis of the rat race ring coupler is developed with its four arms being allowed to have different characteristic impedances. The transmission line theory incorporated with the even-odd analysis is used to formulate the conditions for solving the circuit parameters. The solution shows that a rat race ring with a normalized area of 41.82% or 0.97λ-circumference can be achieved. Based on the solutions, simulated bandwidths of the new ring hybrids are reported. Two experimental circuits are measured for validation check. One uses stepped-impedance sections to realize the four arms for further size reduction. This circuit occupies only 13.12% of that of a conventional hybrid ring at 1 GHz. It is believed that this implementation has the best size reduction for a microstrip ring hybrid in open literature. Measured scattering parameters show good agreement with the simulated results.

Received 17 July 2010, Accepted 2 September 2010, Scheduled 9 September 2010
Corresponding author: J.-T. Kuo (jtkuo123@mail.cgu.edu.tw).

1. INTRODUCTION

Power dividers [1–3] and couplers [4–6] are fundamental and important passive circuits in RF/microwave front end. They can be incorporated with triplexers [1], balanced mixers and balanced amplifiers for equal or unequal power division [2, 3].

Recently, circuit miniaturization has been a hot research topic for passive microwave devices, e.g., couplers [4–6], antennas [7], and filters [8]. For a rat race ring coupler, when frequency is low, the circuit can be unacceptably large since its circumference is $3\lambda/2$ long, where λ is wavelength at the operation frequency. To reduce the circuit size, the most intuitive way is to fold the line traces. The folded structure in [4] has four- to five-fold reduction in footprint as compared with the conventional ring hybrid. Incorporation of lumped elements into the coupler is also quite effective for size reduction. In [5], distributed capacitors are placed within the empty space of the hybrid. It shows a size reduction by 62% compared with the conventional 3-dB branch-line hybrid coupler while providing similar performance and bandwidth. The inductors in [6], however, typically have a low quality factor and will degrade the circuit performance.

Many effective approaches have been reported for miniaturizing distributed rat race couplers. The designs based on the photonic bandgap cells [9] and the compensated spiral compact microstrip resonant cells [10] consume normalized areas of only 60% and 45%, respectively. In [10–13], phase inverters of $\lambda/4$ long are used to replace the $3\lambda/4$ section, so that the normalized area can be reduced to $(2/3)^2 \approx 44.4\%$. Embedding the patterned apertures in the ground plane under the peripheral of the hybrid can save 64% of the circuit area [14]. The lumped distributed approach in [15] results in a size reduction of 55.2%. The idea is close to the slow wave effect produced by attaching periodical capacitive loads to transmission line sections in [16].

In [17], $\lambda/8$- and $\lambda/6$-sections are proposed to design 3-dB hybrid-ring couplers with $5\lambda/4$ and $7\lambda/6$ circumferences, respectively. The area of the $7\lambda/6$-ring uses about 60% of that of the conventional 1.5λ-ring. In [18], the four sections of the $7\lambda/6$-ring [17] are miniaturized by the stepped-impedance configurations. The circuit shows a normalized area of 21% and no passband up to the sixth harmonic. In addition to size reduction, the stepped-impedance configuration is suitable for dual-band design, e.g., [19] where the 2.45/5.2 GHz rat race couplers use only a normalized area of about 21% at the first band. In [20], a rat-race coupler with a peripheral of close to 1λ is achieved, and a $19\lambda/18$-ring is realized and measured at 0.9 GHz. In their formulation,

the four sections have identical characteristic impedance and three of them are commensurate. In [21], design formulas for a generalized 180° hybrid coupler are presented.

This paper extends the derivation in [20] and [21] to a more generalized or detailed fashion. The extension includes that the four arms may have different characteristic impedances and that the three shorter arms may have different lengths. Design equations are derived for calculating the circuit parameters based on the transmission line theory. The solutions show that the circuit circumference can be further reduced to less than 1λ. Based on the solution, size reduction factors and simulation bandwidths for reduced-length couplers are investigated and discussed. In addition, the approach in [18] is employed to replace the four arms at 1 GHz, and it results in a normalized circuit area of 13.12% or 0.54λ-circumference. In the following, formula will be derived for synthesizing the peripheral of ring hybrids. Some solutions are presented and the corresponding circuit bandwidths are discussed. Measured results of experimental circuits are compared with simulation data for validation of the theory.

2. FORMULATION

Figure 1 shows the layout of the rat race ring under investigation with port designation. The reference port admittance is normalized to unity. The parameters θ_i and Y_i (i = 1, 2 and 3) denote the electric length and characteristic admittance of the section, respectively. Based on the even-odd analysis, the four-port network can be reduced to a two-port shown in Fig. 2. Let jY_a and jY_b be respectively the input admittances

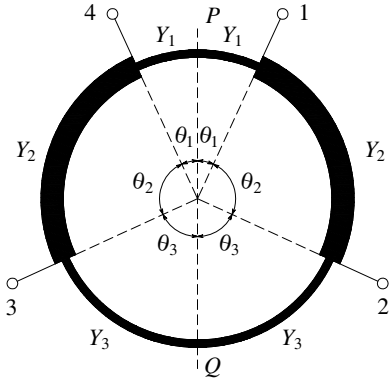

Figure 1. Schematic of the rat race coupler under analysis.

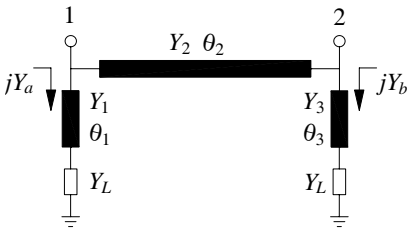

Figure 2. Reduced circuit for even- and odd-mode analysis.

seen at ports 1 and 2 looking into the sections loaded with Y_L. The $ABCD$ matrix of the two-port in Fig. 2 can be derived as

$$A = \cos\theta_2 - \frac{Y_b}{Y_2}\sin\theta_2 \tag{1a}$$

$$B = \frac{j\sin\theta_2}{Y_2} \tag{1b}$$

$$C = j\cos\theta_2\,(Y_a + Y_b) + j\sin\theta_2\left(Y_2 - \frac{Y_aY_b}{Y_2}\right) \tag{1c}$$

$$D = \cos\theta_2 - \frac{Y_a}{Y_2}\sin\theta_2 \tag{1d}$$

when $Y_L = 0$, i.e., the even mode, $Y_a = Y_1\tan\theta_1$ and $Y_b = Y_3\tan\theta_3$. When excitation is taken at port 1, the reflection and transmission coefficients can be derived as

$$\Gamma_e = \frac{A + B - C - D}{A + B + C + D} \equiv \frac{E_3 + jE_4}{E_1 + jE_2} \tag{2a}$$

$$T_e = \frac{2}{A + B + C + D} \equiv \frac{2}{E_1 + jE_2} \tag{2b}$$

where

$$E_1 = \cos\theta_2\left(2 - \tan\theta_2\left(\frac{Y_1}{Y_2}\tan\theta_1 + \frac{Y_3}{Y_2}\tan\theta_3\right)\right) \tag{3a}$$

$$E_2 = \cos\theta_2\left(\frac{\tan\theta_2}{Y_2} + \Delta\right) \tag{3b}$$

$$E_3 = \sin\theta_2\left(\frac{Y_1}{Y_2}\tan\theta_1 - \frac{Y_3}{Y_2}\tan\theta_3\right) \tag{3c}$$

$$E_4 = \cos\theta_2\left(\frac{\tan\theta_2}{Y_2} - \Delta\right) \tag{3d}$$

$$\Delta = Y_1\tan\theta_1 + Y_3\tan\theta_3 + \tan\theta_2\left(Y_2 - \frac{Y_1Y_3}{Y_2}\tan\theta_1\tan\theta_3\right) \tag{3e}$$

For the odd mode, $Y_L = \infty$ and the two coefficients can be derived in a similar fashion. Let

$$\Gamma_o = \frac{X_3 + jX_4}{X_1 + jX_2} \tag{4a}$$

$$T_o = \frac{2}{X_1 + jX_2} \tag{4b}$$

where X_k is E_k (k = 1, 2, 3 and 4) by replacing $\tan\theta_1$ and $\tan\theta_3$ with $-\cot\theta_1$ and $-\cot\theta_3$, respectively. Since the coupler is reciprocal

and symmetric about the PQ plane, only six entries of its 4×4 S-parameter matrix, i.e., S_{m1} ($m = 1$, 2, 3 and 4), S_{22} and S_{32} have to be derived. When excitation is taken at port 2, it can be validated that the reflection and transmission coefficients are the results in (2) and (4) by interchanging the indices 1 and 3.

Next, the following inter-port properties are used to formulate the conditions for solving the circuit parameters:

1) S_{31} (isolation) $= (T_e - T_o)/2 = 0 \Rightarrow E_1 = X_1$ and $E_2 = X_2$. It leads to $Y_1(\tan\theta_1 + \cot\theta_1) + Y_3(\tan\theta_3 + \cot\theta_3) = 0$ and $\tan^2\theta_1 \tan^2\theta_3 = 1$, so that

$$Y_3 = Y_1 \tag{5a}$$

$$\theta_3 = \theta_1 \pm \frac{n\pi}{2}, \quad n = 1, 3, 5, \ldots \tag{5b}$$

2) S_{11} (input matching) $= (\Gamma_e + \Gamma_o)/2 = 0 \Rightarrow E_3 = -X_3$ and $E_4 = -X_4$. The same conditions are obtained when $S_{22} = 0$ is used.

3) $S_{21} = (T_e + T_o)/2 = S_{41} = (\Gamma_e - \Gamma_o)/2$ (in-phase outputs) $\Rightarrow E_3 = X_3 + 4$ and $E_4 = X_4$. The same conditions are obtained when the out-of-phase condition $S_{12} = -S_{32}$ is applied.

Based on the results of properties 2) and 3), we have $E_3 = 2$, $X_3 = -2$ and $E_4 = X_4 = 0$. The following conditions can then be obtained:

$$\sin\theta_2 = R\sin 2\theta_1 \tag{6}$$

$$\left(1 - Y_1^2 - Y_2^2\right)\tan\theta_2 + 2Y_1Y_2\cot 2\theta_1 = 0 \tag{7}$$

where $R = Y_2/Y_1$. In (5b), the solution of the minus sign is just that of the plus sign with interchange of θ_1 and θ_3 (See also Fig. 1). Therefore, choosing the plus sign will not lose any solution since $Y_1 = Y_3$, as shown in (5a). Furthermore, for minimizing the ring size, $n = 1$ is used herein. Based on (6), Fig. 3(a) plots the solution θ_2 versus θ_1 for various R values. One can see that for any θ_1 there are two θ_2 solutions, and vice versa. Note that the solution curves in Fig. 3(a) are bisymmetric about $\theta_1 = 45^\circ$ and $\theta_2 = 90^\circ$. For circuit size miniaturization, only the results in the region of $\theta_1 \leq 45^\circ$ and $\theta_2 \leq 90^\circ$ will be considered herein. Similarly, when $R = 1$ we choose $\theta_2 = 2\theta_1$ instead of $\theta_2 = \pi - 2\theta_1$ as the solution to (6). Substituting (6) into (7), we have

$$\frac{1}{Y_1} = \sqrt{1 + R^2 - 2R\cot 2\theta_1 \cot\theta_2} \tag{8}$$

when $R = 1$, it can be readily derived that

$$\frac{1}{Y_1} = \sqrt{2\left(1 - \cot^2 2\theta_1\right)} \tag{9}$$

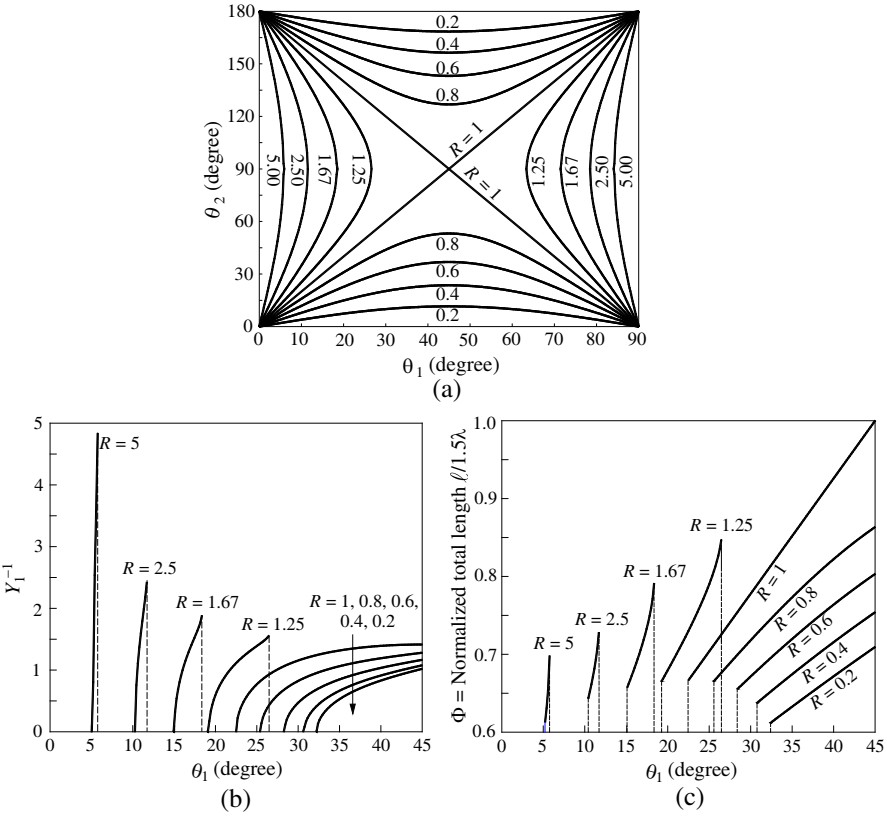

Figure 3. (a) θ_2 and (b) Y_1^{-1} solutions as functions of θ_1 for various R values. (c) Normalized total circumference. The θ_1 and θ_2 values are the electric lengths of the sections evaluated at the operation frequency.

which is identical to that given in [20], where all the solutions to the ring hybrid design are in one curve. One can validate that (6) and (8) are equivalent to (1a) and (1b) of [21]. It should be noted that the condition that θ_1 and θ_2 have to obey in (2) of [21] is an inequality. Here, it has an explicit form in (6) and is plotted in Fig. 3(a). Based on (8), Fig. 3(b) plots the $Z_1 = Y_1^{-1}$ solutions against θ_1. For each R value, the real Z_1 solution exists only within a certain θ_1 range. By enforcing $Z_1 = 0$ in (8), it can be derived that the lower θ_1 bound can be calculated by

$$\sin 2\theta_1 = \frac{\sqrt{2}}{|1 - R^2|}\sqrt{\sqrt{2(1 + R^4)} - (1 + R^2)} \tag{10}$$

For example, when $R = 5$ and 0.2, the lower bounds are $\theta_1 = 5.20°$

and 32.25°, respectively. For the particular case of $R = 1$, $\theta_1 = 22.5°$ can be easily obtained by enforcing $\cot 2\theta_1 = 1$ in (9) or by evaluating (10) using the L'Hospital's rule. When Z_1 is a small number, say 0.2, the θ_1 value will be close to that given in (10) since each curve has a large slope when $Z_1 = 0$. The Z_1 solution curves for $R \geq 1$ have various upper bounds which are also functions of R and can be derived from (6):

$$\theta_1 = \sin^{-1}\left(R^{-1}\sin\theta_2\right)/2 \leq \sin^{-1}\left(R^{-1}\right)/2 \tag{11}$$

For example, when $R = 5$ and 1.25, the upper bounds are $\theta_1 = 5.77°$ and 26.57°, respectively. When $R \leq 1$, the upper θ_1 bounds can be calculated from the corresponding lower bound in (10) since the Y_1^{-1} curves are symmetric about $\theta_1 = 45°$.

Based on (5b) and (6), the total circumference of the ring can be expressed in terms of θ_1 as

$$\Phi(\theta_1) = 4\theta_1 + 2\sin^{-1}(R\sin 2\theta_1) + 180° \tag{12}$$

Figure 3(c) plots the total length ℓ of the hybrid ring normalized with respect to 1.5λ, or

$$\underline{\Phi} = \Phi(\theta_1)/540° \tag{13}$$

for the given R values. Note that as compared with the traditional 1.5λ-ring, the normalized area is square of $\underline{\Phi}$.

One can design the circuit starting from a given size reduction, e.g., $\underline{\Phi} = 0.7$, and Fig. 3(c) shows that there are many possible R values. Alternatively, the design can start from a given θ_1, say $\theta_1 = 30° > 22.5°$, a smaller R value will lead to a better area reduction. Note that when $R = 1$, as in [20], the best theoretical size reduction is $\ell = \lambda$ (normalized area = 4/9) under the limit of $Y_1^{-1} = 0$ where $\theta_1 = 22.5°$. If Y_2 is different from Y_1, i.e., $R \neq 1$, a hybrid ring with $\ell < \lambda$ can be obtained. It is also possible to start the design from a given Y_1^{-1} in Fig. 3(b). Once the θ_1 and R values are chosen, θ_2 can be determined by invoking the solution curves in Fig. 3(a).

3. SIMULATION AND MEASUREMENT

Figure 4 compares simulation and measured responses of a rat race coupler, built on a substrate with $\varepsilon_r = 2.2$ and thickness = 0.508 mm, with $\ell = 0.97\lambda$ at $f_o = 2.5$ GHz. The ring has a mean radius of 13.47 mm and a normalized area of $(0.97/1.5)^2 = 41.82\%$. Some important circuit parameters are $\theta_1 = 9.4°$, $\theta_2 = 65.8°$, $\theta_3 = 99.4°$, and $R = 2.83$. The simulation is done by the IE3D [22]. The magnitude responses are in Fig. 4(a), and the relative phases in Fig. 4(b). At f_o, the measured $|S_{11}|$, $|S_{21}|$, $|S_{31}|$ (isolation) and $|S_{41}|$ are -21.4 dB,

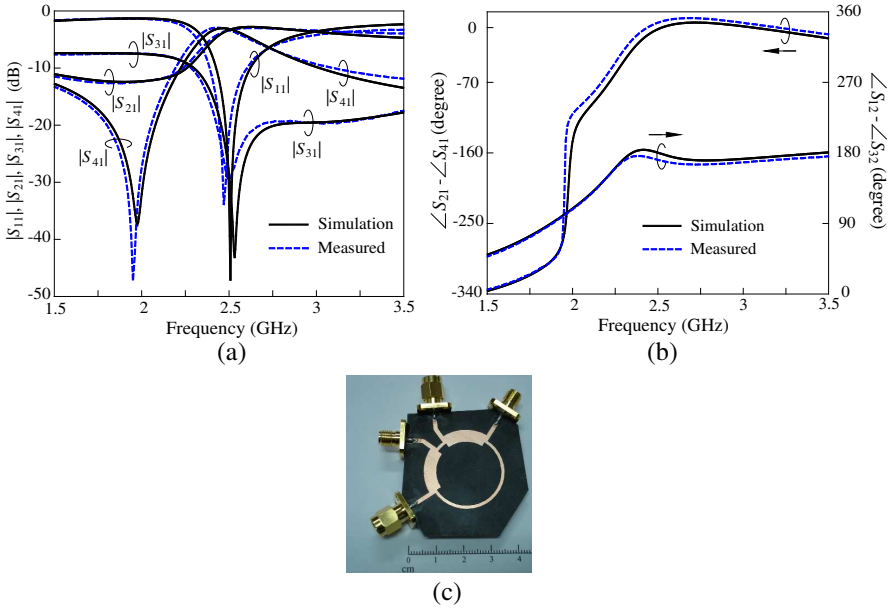

Figure 4. Performances of the experimental rat race coupler. (a) Magnitude responses. (b) Phase responses. (c) Photograph of the circuit. $Y_1^{-1} = 62.15\,\Omega$ ($W_1 = 1.09\,\text{mm}$), $Y_2^{-1} = 21.96\,\Omega$ ($W_2 = 4.64\,\text{mm}$), $\theta_1 = 9.4°$, $\theta_2 = 65.8°$, $\theta_3 = 99.4°$.

$-3.37\,\text{dB}$, $-29.56\,\text{dB}$ and $-3.36\,\text{dB}$, respectively. The best measured $|S_{11}|$ is $-33.9\,\text{dB}$ at $2.47\,\text{GHz}$. The measured results show good agreement with the simulation. Fig. 4(c) shows the photo of the measured circuit.

Figure 5 plots the simulation bandwidths of the new rat race rings. Although the entire circuit has four stepped-impedance junctions, only the circuits with $R = 5$ and 0.2 need slight trimming for tuning the $|S_{31}|$ dips at $f_o = 2.5\,\text{GHz}$. A ring with $R = 0.2$ is used for test the circuit bandwidth. The parameters are $\theta_1 = 33.8°$, $\theta_2 = 10.7°$, $\theta_3 = 123.8°$, $Y_1^{-1} = 20.48\,\Omega$ and $Y_2^{-1} = 102.39\,\Omega$. The bandwidths measured by $|S_{11}| = -15\,\text{dB}$, $|S_{31}| = -20\,\text{dB}$, $|S_{12}/S_{32}| = \pm 0.5\,\text{dB}$, $|S_{21}/S_{41}| = \pm 0.5\,\text{dB}$, $\angle S_{21} - \angle S_{41} = \pm 5°$ and $\angle S_{12} - \angle S_{32} = 180° \pm 5°$ are 6.8%, 28.9%, 24.8%, 8.8%, 8.8% and 8.5%, respectively. The bandwidth by $|S_{11}| = -15\,\text{dB}$ has the smallest value, so that it is used as a basis in Fig. 5 for demonstration. When $\theta_1 \leq 45°$, for a given R value, a larger θ_1 has a larger bandwidth, except for $R = 1$ and $\theta_1 \geq 35°$. For example, when $R = 1.25$, the bandwidth changes

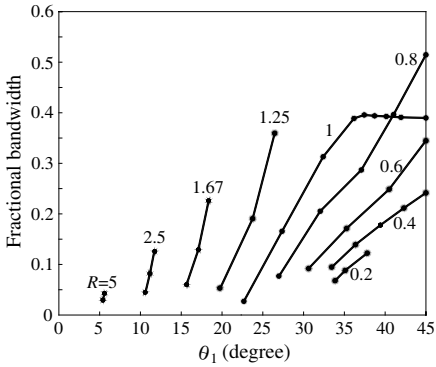

Figure 5. Bandwidths of the new rat race couplers. Bandwidth is defined by the frequencies where $|S_{11}| = -15\,\text{dB}$. Substrate: $\varepsilon_r = 2.2$ and thickness $= 0.508\,\text{mm}$.

from 5% to 35% when θ_1 is varied from 20° to 25°. One can see that when R or $1/R$ is larger, the circuit possesses smaller bandwidth. It is interesting to note that a uniform hybrid ring ($R = 1$) can have a bandwidth from about 5% to 40% by choosing a proper θ_1.

To show more details on the tradeoffs between bandwidth and normalized circumference ($\underline{\Phi}$ in (13)), Table 1 summarizes the data shown in Fig. 3(c) and Fig. 5. For the extreme cases of $R = 0.2$ and $R = 5$, some line widths are too small to be accepted for simulation so that not all solutions in Fig. 3(c) are given in Fig. 5 and Table 1. In Table 1, $\underline{\Phi}_L$ and $\underline{\Phi}_H$ denote the lower and upper limits of $\underline{\Phi}$ in our simulation, and Δ_L and Δ_H are their bandwidths, respectively. It is noted that $\underline{\Phi}_L$ and $\underline{\Phi}_H$ will change when the substrate or the design frequency is changed.

The technique in [18] is employed to further miniaturize the hybrid ring in Fig. 4. The four arms are replaced by stepped-impedance substitutes shown in Fig. 6. The electric length of the Y_3-section is longer than 90°, so that it is replaced with a cascade of two identical stepped-impedance sections. Each substitute has two low-impedance (Z_L) sections at both ends and a high-impedance (Z_H) section in between. The equivalence is established by equating their two-port parameters at the design frequency. It can be validated that to minimize its total length, the length of the Z_H-section is twice of those of the low-impedance ones ($\theta_H = \theta_L$) and can be analytically expressed in terms of the impedance ratio $r = Z_H/Z_L$ [18]. Note that both Z_H and Z_L can be calculated when r and θ_H are given. In general, a larger r value will lead to a better circuit reduction. The size reduction, however, cannot be arbitrary since not only the realizable value of r

is limited by the resolution of the fabrication process but also the ring area limits the realizable width of the Z_L-section. When the substrate dielectric constant or the design frequency is increased, the ring area becomes smaller and hence the size reduction factor.

Figures 7(a) and 7(b) show the performances of a fabricated circuit designed at 1.03 GHz. The values of θ_L $(= \theta_H)$, Z_L and Z_H for the four arms are in Table 2. The length of the Y_1-section of the circuit in Fig. 4 is $2\theta_1 = 18.8°$, and the total length of the stepped-impedance section is only $4\theta_L = 13.2°$. Similarly, Y_2-section (65.8°) and Y_3-section (198.8°) are replaced by their substitutes of total lengths 39.2° and 104°, respectively. Thus the stepped-impedance sections contribute an area reduction factor of $(195.6°/349.2°)^2 = 31.4\%$. The total circumference is 0.54λ and the normalized circuit area is only 13.12%. The size reduction is much better than that of the $7\lambda/6$-ring in [18] and believed to be the best miniaturization of planar rat race couplers in open literature. The measured $|S_{11}|$, $|S_{21}|$, $|S_{31}|$ and $|S_{41}|$ are −22.5 dB, −3.34 dB, −25 dB and −3.56 dB, respectively. The

Table 1. Tradeoffs between bandwidth and normalized circumference of the rat race coupler.

R	$\underline{\Phi}$ (See (13))		Δ(%, $\lvert S_{11}\rvert = -15$ dB)	
	$\underline{\Phi}_L$	$\underline{\Phi}_H$	Δ_L	Δ_H
0.2	0.62	0.65	6.80	12.2
0.4	0.66	0.75	9.50	24.2
0.6	0.68	0.80	9.20	34.5
0.8	0.68	0.86	7.70	51.5
1.0	0.67	1.00	2.70	39.0
1.25	0.68	0.85	5.40	36.0
1.67	0.67	0.79	6.10	22.6
2.5	0.65	0.73	4.50	12.6
5.0	0.63	0.65	2.90	4.50

Table 2. θ_L, Z_L and Z_H of the stepped-impedance sections for substituting the arms of the rat race coupler in Fig. 7.

Section	$\theta_L = \theta_H$	Z_L (Ω)	W_L (mm)	Z_H (Ω)	W_H (mm)
Y_1	3.3°	25.4	3.89	149.0	0.15
Y_2	9.8°	6.6	18.03	55.0	1.35
Y_3	13.0°	13.5	8.24	134.6	0.21

best isolation ($|S_{31}|$) is -35.5 dB at 1.01 GHz. The measured responses are in good agreement with the simulation data. Fig. 7(c) shows the photo of the experimental rat race coupler. The final circuit may look similar to those in [5] and [15], but the approach is quite different. Note that the stepped-impedance section in Fig. 6 consists of one high-impedance section in the middle and in series connection with two low-impedance sections on both sides. The two low-impedance sections are treated as series transmission line sections, neither a capacitor within empty space of the hybrid [5] nor shunt stubs along the main line [15]. When the frequency of the design in Fig. 7 is increased to 2.5 GHz, the total stepped-impedance peripheral becomes 0.78λ and the normalized circuit area is increased to 27.2%, since the ring area limits the line width of the low-impedance sections.

Table 3 compares the bandwidths of the conventional 1.5λ ring, the 0.97λ rat race in Fig. 4, and the 0.54λ and 0.78λ circuits in Fig. 7. The leading three circuits are designed at 2.5 GHz. The circuit in Fig. 4 offers smaller bandwidths than the traditional rat race coupler. In particular, the bandwidths measured by $|S_{11}| = -15$ dB and $|S_{31}| = -20$ dB of the circuit in Fig. 4 are about respectively one tenth and one third of those of the 1.5-λ ring. The reference levels for defining bandwidths of return loss and isolation can be referred to [11]. The simulation bandwidths measured by $\angle S_{41} - \angle S_{21} = \pm 5^\circ$ and $\angle S_{12} - \angle S_{32} = 180^\circ \pm 5^\circ$ of the 0.78λ circuit and that in Fig. 4 are between 4.4% and 12.4%. A comparison of the data of 0.54λ and

Table 3. Bandwidths of the conventional 1.5λ-ring the 0.97λ-rat race in Fig. 4, and the 0.78λ- and 0.54λ-circuits in Fig. 7.

Circuit (2.5 GHz)	$\|S_{11}\| = -15$ dB (Input matching)		$\|S_{31}\| = -20$ dB (Isolation)		$\angle S_{41} - \angle S_{21} = \pm 5^\circ$		$\angle S_{12} - \angle S_{32} = 180^\circ \pm 5^\circ$	
	Sim.	Mea.	Sim.	Mea.	Sim.	Mea.	Sim.	Mea.
1.5λ-ring	39.5%	-	31.3%	-	16.1%	-	15.3%	-
0.97λ-ring	3.9%	4.0%	11.9%	9.4%	5.7%	2.9%	10.8%	2.9%
0.78λ-ring	3.2%	-	5.2%	-	12.4%	-	4.4%	-
0.54λ-ring (1 GHz)	4.6%	3.9%	6.3%	5.9%	16.7%	15.5%	7.2%	9.1%

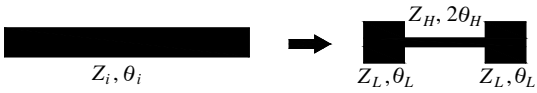

Figure 6. Substitution of a uniform section by a stepped-impedance section for circuit miniaturization.

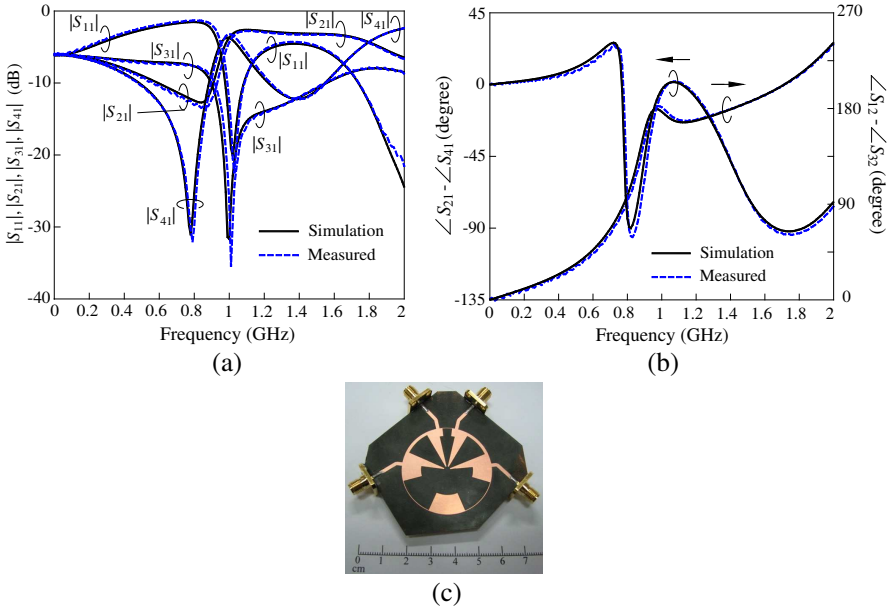

Figure 7. Performances of the 0.54λ-ring coupler. (a) Magnitude responses. (b) Relative phase responses. (c) Photograph of the experimental rat race coupler. Geometric parameters are in Table 3.

0.78λ in Fig. 7 shows that ring miniaturized by the stepped-impedance approach at a lower frequency has larger simulation bandwidths.

4. CONCLUSION

A generalized synthesis for rat race coupler is performed and applied to circuit miniaturization. Design equations are provided for calculating the electric lengths and the characteristic impedances of the four arms. There are two degrees of freedom in choosing the geometric parameters for synthesis of the rat race couplers. The upper and lower bounds of the solutions are given in analytical expressions. Operation bandwidths of the newly synthesized miniaturized rat race couplers are simulated and discussed. A 0.97λ-ring operating at 2.5 GHz is fabricated and measured. The rat race is further reduced by replacing the four arms with stepped-impedance sections at 1 GHz. The circuit occupies only 13.12% of the area of a conventional 1.5λ-ring and its performances are compared with the 0.97λ-ring and the conventional rat race. In general, the size reduction leads to a decreased circuit bandwidth.

ACKNOWLEDGMENT

This work was supported by the National Science Council, Taiwan, under Grant NSC 98-2211-E-009-032-MY2.

REFERENCES

1. Ruiz-Cruz, J. A., J. R. Montejo-Garai, J. M. Rebollar, and S. Sobrino, "Compact full Kuband triplexer with improved E-plane power divider," *Progress In Electromagnetics Research*, Vol. 86, 39–51, 2008.
2. Wu, Y., Y. Liu, and S. Li, "Dual-band modified Wilkinson power divider without transmission line stubs and reactive components," *Progress In Electromagnetics Research*, Vol. 96, 9–20, 2009.
3. Wu, Y., Y. Liu, and S. Li, "An unequal dual-frequency Wilkinson power divider with optional isolation structure," *Progress In Electromagnetics Research*, Vol. 91, 393–411, 2009.
4. Settaluri, R. K., G. Sundberg, A. Weisshaar, and V. K. Tripathi, "Compact folded line rat-race hybrid couplers," *IEEE Microw. Guided Wave Lett.*, Vol. 10, No. 2, 61–63, Feb. 2000.
5. Jung, S.-C., R. Negra, and F. M. Ghannouchi, "A design methodology for miniaturized 3-dB branch-line hybrid couplers using distributed capacitors printed in the inner area," *IEEE Trans. Microw. Theory Tech.*, Vol. 56, No. 12, 2950–2953, Dec. 2008.
6. Hirota, T., A. Minakawa, and M. Muraguchi, "Reduced-size branch-line and rat-race hybrids for uniplanar MMICs," *IEEE Trans. Microw. Theory Tech.*, Vol. 38, No. 3, 270–275, Mar. 1990.
7. Adam, H., A. Ismail, M. A. Mahdi, M. S. Razalli, A. R. H. Alhawari, and B. K. Esfeh, "Xband miniaturized wideband bandpass filter utilizing multilayered microstrip hairpin resonator," *Progress In Electromagnetics Research*, Vol. 93, 177–188, 2009.
8. Li, J.-F., B.-H. Sun, H.-J. Zhou, and Q.-Z. Liu, "Miniaturized circularly-polarized antenna using tapered meander-line structure," *Progress In Electromagnetics Research*, Vol. 78, 321–328, 2008.
9. Shum, K. M., Q. Xue, and C. H. Chan, "A novel microstrip ring hybrid incorporating a PBG cell," *IEEE Microw. Wireless Compon. Lett.*, Vol. 11, No. 6, 258–260, Jun. 2001.
10. Gu, J. and X. Sun, "Miniaturization and harmonic suppression rat-race coupler using C-SCMRC resonators with distributive

equivalent circuit," *IEEE Microw. Wireless Compon. Lett.*, Vol. 15, No. 12, 880–882, Dec. 2005.

11. Fan, L., C.-H. Ho, S. Kanamaluru, and K. Chang, "Wide-band reduced-size uniplanar magic-T, hybrid-ring, and de Ronde's CPW-slot couplers," *IEEE Trans. Microw. Theory Tech.*, Vol. 43, No. 12, 2149–2158, Dec. 1995.
12. Wang, T. and K. Wu, "Size-reduction and band-broadening design technique of uniplanar hybrid ring coupler using phase inverter for M(H)MIC's," *IEEE Trans. Microw. Theory Tech.*, Vol. 47, No. 2, 198–206, Feb. 1999.
13. Kao, C.-W. and C.-H. Chen, "Novel uniplanar 180° hybrid-ring couplers with spiral-type phase inverters," *IEEE Microw. Guided Wave Lett.*, Vol. 10, No. 10, 412–414, Oct. 2000.
14. Sung, Y. J., C. S. Ahn, and Y.-S. Kim, "Size reduction and harmonic suppression of rat-race hybrid coupler using defected ground structure," *IEEE Microw. Wireless Compon. Lett.*, Vol. 14, No. 1, 7–9, Jan. 2004.
15. Chun, Y.-H. and J.-S. Hong, "Compact wide-band branch-line hybrids," *IEEE Trans. Microw. Theory Tech.*, Vol. 54, No. 2, 704–709, Feb. 2006.
16. Eccleston, K. W. and S. H. M. Ong, "Compact planar microstripline branch-line and rat-race coupler," *IEEE Trans. Microw. Theory Tech.*, Vol. 51, 2119–2125, Oct. 2003.
17. Kim, D. I. and G. S. Yang, "Design of new hybrid-ring directional coupler using $\lambda/8$ or $\lambda/6$ sections," *IEEE Trans. Microw. Theory Tech.*, Vol. 39, No. 10, 1779–1783, Oct. 1991.
18. Kuo, J.-T., J.-S. Wu, and Y.-C. Chiou, "Miniaturized rat race coupler with suppression of spurious passband," *IEEE Microw. Wireless Compon. Lett.*, Vol. 17, No. 1, 46–48, Jan. 2007.
19. Hsu, C.-L., J.-T. Kuo, and C.-W. Chang, "Miniaturized dual-band hybrid couplers with arbitrary power division ratios," *IEEE Trans. Microw. Theory Tech.*, Vol. 57, No. 1, 149–156, Jan. 2009.
20. Mandal, M. K. and S. Sanyal, "Reduced-length rat-race couplers," *IEEE Trans. Microw. Theory Tech.*, Vol. 55, No. 12, 2593–2598, Dec. 2007.
21. Murgulescu, M.-H., E. Penard, and I. Zaquine, "Design formulas for generalised 180° hybrid ring couplers," *Electron. Lett.*, Vol. 30, No. 7, 573–574, Mar. 1994.
22. *IE3D Simulator*, Zeland Software Inc., Jan. 1997.